Published online 22 July 2019

Nucleic Acids Research, 2019, Vol. 47, No. 15 ***7767–7780***
doi: 10.1093/nar/gkz620

DNA complexes with human apurinic/apyrimidinic endonuclease 1: structural insights revealed by pulsed dipolar EPR with orthogonal spin labeling

Olesya A. Krumkacheva[1,2,3], Georgiy Yu. Shevelev[2,4], Alexander A. Lomzov[2,4], Nadezhda S. Dyrkheeva[4], Andrey A. Kuzhelev[1,2,3], Vladimir V. Koval[2,4], Victor M. Tormyshev[1,2], Yuliya F. Polienko[1,2], Matvey V. Fedin[2,3], Dmitrii V. Pyshnyi[2,4], Olga I. Lavrik[2,4] and Elena G. Bagryanskaya[1,2,*]

[1]N. N. Vorozhtsov Novosibirsk Institute of Organic Chemistry SB RAS, 9 Lavrentiev ave, Novosibirsk 630090, Russia, [2]Novosibirsk State University, Pirogova Str. 2, Novosibirsk 630090, Russia, [3]International Tomography Center SB RAS, Institutskaya Str. 3a, Novosibirsk 630090, Russia and [4]Institute of Chemical Biology and Fundamental Medicine SB RAS, 8 Lavrentiev ave, Novosibirsk 630090, Russia

Received April 24, 2019; Revised July 04, 2019; Editorial Decision July 08, 2019; Accepted July 11, 2019

ABSTRACT

A DNA molecule is under continuous influence of endogenous and exogenous damaging factors, which produce a variety of DNA lesions. Apurinic/apyrimidinic sites (abasic or AP sites) are among the most common DNA lesions. In this work, we applied pulse dipolar electron paramagnetic resonance (EPR) spectroscopy in combination with molecular dynamics (MD) simulations to investigate in-depth conformational changes in DNA containing an AP site and in a complex of this DNA with AP endonuclease 1 (APE1). For this purpose, triarylmethyl (TAM)-based spin labels were attached to the 5′ ends of an oligonucleotide duplex, and nitroxide spin labels were introduced into APE1. In this way, we created a system that enabled monitoring the conformational changes of the main APE1 substrate by EPR. In addition, we were able to trace substrate-to-product transformation in this system. The use of different (orthogonal) spin labels in the enzyme and in the DNA substrate has a crucial advantage allowing for detailed investigation of local damage and conformational changes in AP-DNA alone and in its complex with APE1.

INTRODUCTION

A number of endogenous and exogenous damaging factors continuously affect DNA, leading to a variety of DNA lesions, the most common of which are apurinic/apyrimidinic sites (abasic or AP sites). Nearly 10 000 AP sites are produced daily in a typical human cell (1). Most of them are the result of either spontaneous depurination (1) or deamination of cytosine to uracil, which is then eliminated by uracil DNA glycosylases (2,3). Abasic sites also arise when oxidized or alkylated bases are removed by other specific DNA glycosylases (4–6). Unrepaired AP sites are mutagenic (7). Studies on AP sites within a template for DNA polymerases suggest that they preferentially incorporate dA (deoxyadenosine monophosphate) opposite the AP site (8–10). During translesion DNA synthesis catalyzed by Y-family DNA polymerases, AP sites can also cause frameshifts in the polymerase's product (11,12). *In vivo*, AP sites are thought to be repaired via the DNA base excision repair pathway (BER), which targets damaged bases and spontaneously emerging AP sites. The repair of AP sites via BER is initiated by apurinic/apyrimidinic endonuclease, which excises DNA 5′ from the AP site, resulting in a 3′-hydroxyl group and a 5′-deoxyribose phosphate. In humans, BER initially involves apurinic/apyrimidinic endonuclease 1 (APE1).

In a series of publications, the conformations of DNA containing AP sites have been investigated by nuclear magnetic resonance (NMR), electron paramagnetic resonance (EPR), crystallography and molecular dynamics (MD) simulations (13–21). On many occasions, the researchers have emphasized the importance of the anomeric form (α- or β-hemiacetals) of an AP site and the sequence context (neighboring bases) for the conformation of DNA, which can be intrahelical or more extrahelical and surface accessible, with or without a significant distortion of the DNA backbone opposite the lesion. Furthermore, all the authors in this field note that the DNA damage including the base loss affects the local structure and flexibility of the DNA helix, which

*To whom correspondence should be addressed. Tel: +7 383 330 88 50; Email: egbagryanskaya@nioch.nsc.ru

may be important for the ability of proteins to recognize the lesion sites (22,23).

APE1 is a homolog of *Escherichia coli* exonuclease III, which belongs to the Xth family of AP endonucleases. It is responsible for >95% of the total AP endonuclease activity in a HeLa cell extract (24,25). APE1 is a multifunctional and extremely active enzyme (26,27) and can process various synthetic analogs of the AP site such as 3-hydroxy-2-(hydroxymethyl)tetrahydrofuran (F) and other non-nucleotide insertions modeling AP sites (28,29). F has often been used as a model for an enzymatically generated AP site (27,30,31). Analysis of the publications on structures of free APE1 (32–34) and DNA/APE1 complexes (35–37) produced by different groups shows that there are still some inconsistencies in the understanding of the catalytic function of the enzyme and its interaction with damaged DNA.

The analysis of crystal structures of APE1 (32–34) and of DNA/APE1 complexes (35–37) shows that the DNA helix is bent and that F is extrahelically flipped out of the helix into a specific binding pocket of the protein (35,38). This observation implies penetration of protein side chains into the region adjacent to the AP site (36). Nonetheless, other results contradict these data. Structure-driven mutagenesis studies suggest that APE1 does not actively flip out the deoxyribose into its extrahelical conformation, but the flexibility of the substrate is important for enzymatic recognition (35). Furthermore, APE1 has been demonstrated to process over 200 base pairs or more (39), and the DNA scanning for an AP site lesion involves sensing of DNA flexibility. At the same time, some other studies indicate that this flexibility is not exclusively responsible for the lesion recognition by APE1 (25). Thus, whether the conformation of an AP site in a DNA duplex in solution is inherently perturbed or APE1 alters the DNA structure in the lesion region remains unclear because the conclusions of available studies are often ambiguous or contradictory.

Pulsed dipolar (PD) EPR techniques are based on the measurement of a magnetic dipole–dipole interaction between two spin labels by means of microwave pulses (40–43). Various approaches of PD EPR are actively used, in particular pulsed electron double resonance (PELDOR or DEER) (44) and double quantum coherence (DQC) (45). These methods enable measuring spin–spin distances and their distributions spanning the range of 2 to 10 nm. PELDOR was recently applied in a series of works for investigation of structural characteristics of nucleic acids (46–50) and of DNA containing different types of damage (19–21). These works concluded that PELDOR of spin-labeled DNA molecules could serve as a 'molecular ruler' showing the influence of local damage on the DNA conformations. The authors analyzed the changes in the distances between two nitroxide spin labels attached at the DNA termini. Triarylmethyl (TAM or trityl)-based spin labels represent a potent alternative to nitroxides for EPR distance measurements in biomolecules (51–53). Recently, we reported that double spin-labeling using TAMs allows obtaining narrower spin–spin distance distributions in DNA duplexes and provides higher accuracy of measurement as compared to nitroxide labels (54, 55). Moreover, we have proven that these EPR data are in good agreement with NMR and MD simulation results (56). In general, the comparison of PELDOR using TAMs versus nitroxides reveals substantial advantages of TAM spin-labeling (53,54,57–59).

In the present work, we applied PELDOR (34 GHz, Q-band) using orthogonal spin labeling with TAMs and nitroxides to investigate the conformations of DNA containing an AP site (AP-DNA) and of an AP-DNA/APE1 complex at qualitatively new level. For this purpose, the TAM labels were attached at 5′ ends of an oligonucleotide duplex, while nitroxide spin labels were inserted into APE1. Thus, we for the first time created a benchmark system that enables the following conformational changes of the main APE1 substrate by EPR. Furthermore, the experimentally obtained data and their interpretation were supported and strengthened by MD simulations. Note that in the previous work (19), the authors did not measure the mean distance in an AP-DNA/APE1 complex by PELDOR: they only evaluated it by MD analysis. In addition, in the present work, we were able to trace the substrate-to-product transformation. For the first time, we introduced nitroxide spin labels into APE1; this approach, in conjunction with TAM-labeled DNA, allowed us to perform PELDOR with orthogonal spin labels and to confirm the formation of a DNA/APE1 complex as well as to obtain more information about its structure.

MATERIALS AND METHODS

Recombinant APE1 expression and purification

The recombinant APE1 (APE1_WT) and the mutant APE1 protein (with the N212A substitution), i.e. APE1N212A, were purified as described elsewhere (31). Plasmid pXC53 was kindly provided by Dr S.H. Wilson (NIEHS NIH, NC, USA). We also used the pXC53 plasmid to produce a mutant form of APE1 with the N212A substitution. Briefly, all the proteins were expressed in the *E. coli* BL21DE3 strain. The cells were cultured on a selection medium containing LB/SOC agar with ampicillin (100 μg/ml). Protein expression was started by adding 1 mM isopropyl-β-D-thiogalactoside (IPTG). The cells were lysed, and the cell debris was removed by centrifugation. Next, the target proteins were purified by ion exchange chromatography on HiTrap SP HP (GE Healthcare) and then by affinity chromatography using HiTrap Heparin HP (GE Healthcare) as described previously (31).

The spin labeling of APE1N212A

To carry out spin labeling of the protein, 500 μl of a 50 μM APE1N212A solution in storage buffer (10 mM Tris-HCl, 50 mM KCl, 0.1 mM EDTA, 50% of glycerol, pH 7.5) was concentrated using a 10 kDa Omicon filter (Merck, Germany) in MOPS buffer (50 mM MOPS, 25 mM NaCl, pH 7.4) to final volume 40 μl and protein concentration 500 μM. Then, we added 5 μl of the 3-((2-iodoacetamido)methyl)-2,2,5,5-tetramethyl-2,5-dihydro-1H-pyrrol-1-oxyl (NR) spin label solution (methanol–water, 20%, v/v) in a 10-fold molar excess. NR (2 mg) was dissolved in 10 μl of methanol with 40 μl H_2O. The solution of the spin label was added to the protein solution in two 2.5 μl portions (the second portion was added after 2

h). The reaction was carried out at 10°C for 24 h. The excess of the spin label was removed using a 10 kDa Omicon filter (Merck, Germany) with 3 ml of MOPS buffer. The nitroxide concentration measured in spin-labeled mutant APE1 (SL-APE1N212A) by continuous wave (CW) EPR was 2-fold greater than the protein concentration. Identification of spin-labeled sites within the protein was conducted by proteolytic digestion with subsequent matrix-assisted laser desorption ionization time of flight (MALDI-TOF) tandem mass-spectrometry (MS/MS) analysis. The results are given in Supplementary Data. According to the mass spectrometry data, there are three possible spin-labeled sites, which were identified at the following positions: Cys138 (N1), Cys296 (N3) and Cys310 (N2).

Identification of spin-labeled sites by mass spectrometry

To verify the sequence of APE1 and identify the sites of spin-labeling in APE1N212A, the samples were treated with proteolytic enzyme chymotrypsin in the presence of dithiothreitol (DTT) and iodoacetamide. To this end, 0.3 μl of APE1 (5 μg/μl) or APE1N212A (5 μg/μl) was mixed with 10 μl of 40 mM NH_4HCO_3, 0.2 μl of 1% ProteaseMax (Promega, USA) and 0.6 μl of 0.1 M DTT, and incubated at 56°C for 20 min. After that, if necessary, 0.35 μl of 0.55 M iodoacetamide was added to the reaction mixture and incubated for 15 min at room temperature in the dark. Then, 0.6 μl of a 0.5 μg/μl chymotrypsin (Promega, USA) solution was added and the reaction mixture was stored overnight at 37°C. If iodoacetamide was used, chymotrypsin and ProteaseMax solutions were added after 15 min incubation of the reaction mixture at room temperature in the dark in the presence of iodoacetamide. After enzymatic treatment, the reaction mixtures of proteins were evaporated in a SpeedVac (Labconco, USA) and further purified with ZipTip (Merck Millipore, Germany). Purified reaction mixtures were analyzed on a MALDI-TOF Autoflex Speed mass spectrometer (Bruker Daltonics, Germany) using DHB as a matrix and displaced on an AnchorChip Target plate. Mass spectra were analyzed in FlexAnalysis 3.0 software integrated with mass-spectrometer workstation. The gene sequences of APE1 and APE1N212A determined by Sanger sequencing were used for comparison of theoretical chymotrypsin digestion spectra of unlabeled and labeled protein with experimental spectra. Spectra processing parameters were as follows: S/N (signal-to-noise ratio) 2/1, mass tolerance 0.4 Da and MS/MS tolerance: 0.5 Da. Sequence coverage with unlabeled APE1 was 80.5% and with the spin-labeled protein was 90.3%. During DTT treatment, the nitroxide radical center of the spin label was reduced to hydroxylamine (60,61) giving a +1 Da increment to the spin label residue. This detail was taken into account during molecular mass calculation of spin-labeled peptides. Spin label residues were identified in peptides LSRQCPL, CDSKIRSKAL and GSDHCPITLY with cysteines # 138 (N1), 296 (N3) and 310 (N2), respectively. To identify an amino acid residue that was labeled with nitroxide, peptides were analyzed at MS/MS settings in LIFT mode. The highest score (166) was obtained for peptide LSRQCPL with mass tolerance 1 Da. Two other peptides were identified with score values 8 and 4.18, respectively. It should be noted

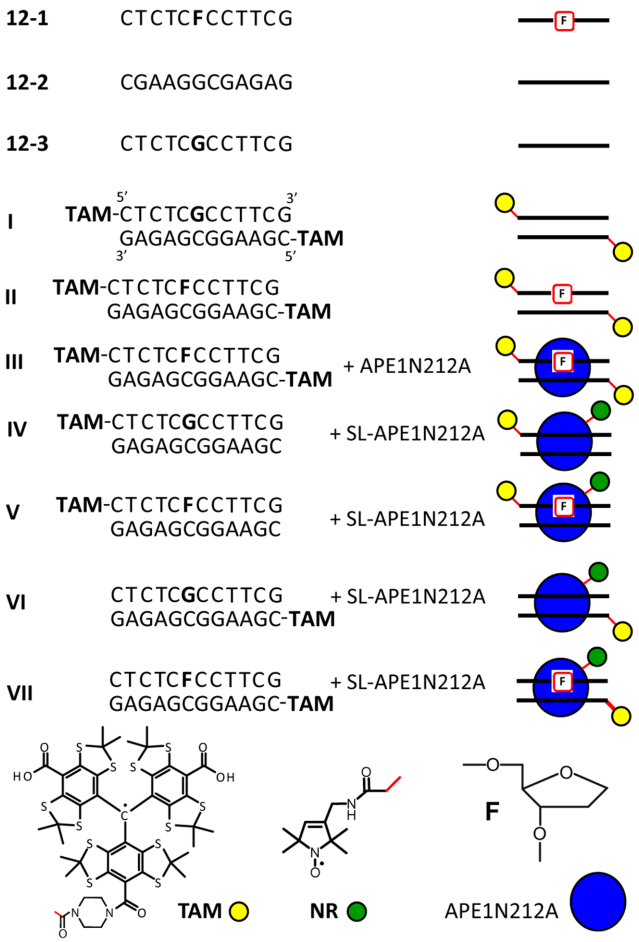

Figure 1. The oligonucleotides and duplexes used for the detection of enzyme binding, for catalytic activity essays and for EPR experiments. F: an AP site analog, tetrahydrofuran or 3-hydroxy-2-hydroxymethyl tetrahydrofuran; TAM, the triarylmethyl spin label. *The 5′-[^{32}P]labeled phosphate group. APE1N212A: mutant form of APE1, SL-APE1N212A: a mutant APE1 spin-labeled with NR.

that the intensity of lines in mass spectra is not directly proportional to the concentration of spin labels at these three analyzed amino acid positions.

The study of APE1 binding and enzymatic activity with AP site-containing TAM-labeled DNA

To study the APE1 enzymatic activity, we synthesized a DNA structure containing an AP site analog, tetrahydrofuran or 3-hydroxy-2-hydroxymethyl tetrahydrofuran (F) with a TAM label at the 5′ end of the complementary strand (*12–1/12–2-TAM, Figure 1) and the control substrate without the spin label (*12–1/12–2, Figure 1). To detect oligonucleotides in a polyacrylamide gel (PAAG), a radioactive ^{32}P label (*) was introduced at the 5′ end of the oligonucleotides by the T4 polynucleotide kinase. Duplexes were formed by heating the mixture of oligonucleotides to 95°C with further gradually cooling to room temperature.

The reaction mixtures contained 100 nM DNA, 50 mM Tris-HCl, pH 8.0, 50 mM NaCl, 7 mM β-mercaptoethanol and APE1 at various concentrations. We added 5 mM

$MgCl_2$ as an enzyme cofactor of the AP endonuclease reaction. The reaction was carried out at 37°C for the period indicated in Supplementary Figure S1 and was stopped by mixing with dyes in formamide. The APE1 reaction products were analyzed by denaturing gel electrophoresis in 20% PAAG with 7 M urea.

During analysis of the formation of DNA/APE1 complexes by a gel shift assay under nondenaturing conditions, 25 mM EDTA was added to the reaction mixture (100 nM DNA, 50 mM Tris-HCl, pH 8.0, 50 mM NaCl, 7 mM β-mercaptoethanol), and the mixture was incubated on ice for 15 min. The formation of DNA/APE1 complexes was analyzed by the separation of free DNA and DNA/protein complexes in a 8% nondenaturing polyacrylamide gel. The visualization of the reaction products and of protein binding was performed using a Typhoon FLA 9500 (GE Healthcare) scanner. The data were analyzed in QuantityOne 4.6.7 software.

Synthesis of spin-labeled oligonucleotides

Oligonucleotides were synthesized using standard synthons for solid-phase phosphoramidite synthesis (Glen Research, USA) with standard protocols. AP non-nucleotide insertion was incorporated into the sequence of an oligonucleotide by dSpacer CE Phosphoramidite synthon 10–1914–02 (Glen Research, USA). Incorporation of the TAM spin label at the 5′ end of a piperazine-labeled oligonucleotide was conducted by a previously described protocol (62). The TAM-labeling of an oligonucleotide was confirmed by CW EPR (Supplementary Figure S3).

Preparation of samples for EPR

Complementary spin-labeled oligonucleotides were mixed in a 10 μl aqueous solution containing 0.25 mM spin-labeled oligonucleotide per each strand, 100 mM NaCl, 2 mM $MgCl_2$ and 10 mM sodium cacodylate (pH 7.0). The solution was dried in a Centrivap vacuum concentrator (Labconco, USA), and after that, the precipitate was dissolved in 10 μl of a 30% d_8-glycerol solution in D_2O (Astrachem, Russia). The sample was immediately vortexed. For introducing a protein into a solution of the DNA complex, the latter was first evaporated, then a 0.25 mM APE1 solution in D_2O was added. Most of the DNA and APE1 formed a complex at the concentrations used, as confirmed by EPR.

EPR experiments

EPR experiments were carried out using a commercial Bruker Elexsys E580 spectrometer equipped with EN5107D2 (Q-band, 34 GHz) resonator and an Oxford Instruments temperature control system. The maximum available microwave power at Q-band was limited to 1 W. Samples were prepared at room temperature in quartz capillary tubes (OD 1.65 mm, ID 1.15 mm, the sample volume ca. 10 μl), shock-frozen in liquid nitrogen and studied at T = 50–80 K.

The DQC measurements were carried out at 80 K by using six-pulse sequence, $\pi/2-\tau_1-\pi-\tau_1-\pi/2-\tau_3-\pi-\tau_3-\pi/2-\tau_2-\pi-\tau_2-$echo (45) with pulse lengths of 24/48 ns (Q-band) for $\pi/2$ and π pulses, respectively. The DQC measurements were carried out at the field position corresponding to the maximum of the EPR spectrum. To filter out unwanted signals, 64-step phase cycling was applied. The DQC time trace was recorded by incrementing τ_1 and decrementing τ_2 in 16 ns steps. The initial values of τ_1 were 3800/4800 ns, the initial values of τ_2 were 4200/5200 ns, and the delay τ_3 = 50 ns remained constant. The number of shots per point was 1, and repetition time was 7.14 ms. The number of points was 250/310, and the total number of scans was 60 for τ_1 = 3800 ns and 200 for τ_1 = 4800 ns. Accumulation time was 3–8 h. All the obtained DQC traces were background-corrected by second- or third-order polynomial functions and analyzed by Tikhonov regularization using DeerAnalysis program (63). DQC experiments on two independently prepared samples showed that the experimental error of distance measurements was <0.1 nm (Supplementary Figure S13).

PELDOR measurements were performed at 50 K using the standard four-pulse, dead time-free PELDOR/DEER sequence (64) with a two-step phase cycle. The repetition time was 3.1 ms. The delay between $\pi/2$ and π pulses was 400 ns. The cycle for suppression of nuclear modulation due to deuterium was applied, in which the delay between the first two pulses was incremented eight times by 16 ns. All experimental PELDOR results were processed using DeerAnalysis 2013 (63).

For PELDOR on pair TAM/TAM the pulse lengths were 24 and 48 ns for $\pi/2$ and π probe pulses (ν_{probe}), respectively, and 50 ns for the π pump pulse (ν_{pump}). The measurements were carried out at a satellite line of low intensity using $\Delta\nu = (\nu_{probe} - \nu_{pump}) = 19$ MHz thus leading to the application of the pump pulse at the spectral maximum. Fifty Kelvin was the optimal temperature for this experimental setup, but a higher temperature (50–80 K) could also be used. The time increment of the inversion pulse was 30 ns. The dipolar evolution time window was 6 μs. The number of shots per point was 10, and the number of points was 190. The number of scans was 220, corresponding to the total accumulation time of ∼9 h.

For PELDOR on pair nitroxide/nitroxide the pulse lengths were 24 and 48 ns for $\pi/2$ and π probe pulses (ν_{probe}), respectively, and 100 ns for the π pump pulse (ν_{pump}). The measurements were carried out at the nitroxide line using $\Delta\nu = (\nu_{probe} - \nu_{pump}) = 60$ MHz leading to application of the pump pulse at the spectral maximum. The time increment of the inversion pulse was 10 ns. The dipolar evolution time window was 5 μs. The number of shots per point was 10, and the number of points was 500. The number of scans was 50, corresponding to the total accumulation time of ∼8 h. The maximal modulation depth for the nitroxide/nitroxide pair at these settings was ∼6.5%, as verified by means of a model DNA duplex double-labeled with nitroxides (54).

For PELDOR on pair nitroxide/TAM pulse lengths were 30 and 60 ns for $\pi/2$ and π probe pulses (ν_{probe}), respectively, and 62 ns for the π pump pulse (ν_{pump}). The measurements were carried out at the nitroxide line using $\Delta\nu = (\nu_{probe} - \nu_{pump}) = 45$ MHz leading to application of the

pump pulse at an intense TAM line. The time increment of the inversion pulse was 20 ns. The dipolar evolution time window was 7 μs. The number of shots per point was 5, and the number of points was 350. The number of scans was 200, corresponding to the total accumulation time of ∼5 h. The maximal modulation depth for the nitroxide/TAM pair at these settings was ∼24%, as verified using a model DNA duplex double-labeled by TAM and nitroxide (54).

The MD simulation

The structure and dynamics of the double-spin-labeled DNA duplexes, spin-labeled protein APE1N212A, and the complex of spin-labeled protein APE1N212A and the double-spin-labeled DNA duplex containing the AP site were studied by MD simulations. The initial structures of duplexes without spin labels were generated with the NAB module of the Amber16 software. The initial structure of the complex of APE1N212A with the AP site DNA duplex was taken from (65). The cysteine residue with the attached nitroxide spin label was optimized by quantum chemical methods in HF/6–31G* by means of Gaussian'09 software. Based on the obtained structures and the electron density distribution, partial charges of atoms were calculated by the RESP method, and MD libraries were created as described in (62). Using the latter, a modified APE1N212A and a complex of APE1N212A with AP site DNA bearing the nitroxide and TAM spin labels were created by introduction of nitroxide spin labels at cysteine residues 138, 296 and 310. It was assumed that the spin labels did not directly interact with each other, thus allowing us to determine the distance between the TAM labels in the DNA duplex and between the TAM labels in DNA and the nitroxide label in the protein in one series of MD experiments. The structure of the spin-labeled duplexes, of the protein, and of the complex was relaxed, and simulation was performed by the MD method. The simulation was carried out by means of the AMBER16 software package using the pmemd.CUDA program, with the parmbsc0 force field for DNA, ff14SB for the protein part of the complex and gaff parameters for modified fragments. The analysis was carried out in explicit TIP3P water models as described in (66). The MD experiment in an implicit solvent shell provides more complete coverage of the conformation space, whereas the experiment with an explicit solvent shell ensures more reliable results of the simulation and is more time consuming. The analysis of the trajectories was performed in the cpptraj software, and visualization was carried out in UCSF Chimera (USA).

RESULTS

The detailed structural studies of AP-DNA/APE1 complexes by pulsed dipolar EPR require several consecutive steps. First, the enzymatic activity of spin-labeled DNA and protein needs to be compared with unmodified analogs to ensure that biological functions were not perturbed. Next, spin-labeled components of the complexes have to be studied by EPR to provide a reference in the absence of any mutual interactions. Finally, target complexes of spin-labeled components should be investigated using PD EPR. In the sections below, we describe our studies which follow this strategy.

Enzymatic activity of APE1, of the mutant protein APE1, and of spin-labeled mutant APE1

We investigated the enzymatic activities of APE1, of the mutant protein APE1N212A, and of spin-labeled mutant SL-APE1N212A in a model AP-DNA structure with a spin label (*12–1/12–2-TAM) and compared the results with the control AP-DNA structure (*12–1/12–2) without a spin label. We analyzed the substrate (S, Supplementary Figure S1) consumption and product (P, Supplementary Figure S1) formation during the reaction by separating the substrate and product by denaturing gel electrophoresis in PAAG. The control mixtures with the substrates without the addition of the enzyme were run in lanes 1 and 10 (Supplementary Figure S1A). Wild-type APE1 incises the model AP site in DNA with the spin label (*12–1/12–2-TAM, Supplementary Figure S1A, lanes 11–14) less efficiently as compared to the control substrate without a spin label (Supplementary Figure S1A, lanes 2–5). Supplementary Figure S1B presents data on the efficiency of formation of an endonuclease reaction product during the reaction. The rate of AP site hydrolysis catalyzed by APE1 in the control unlabeled substrate was higher than that in the spin-labeled substrate. This is possibly due to the steric hindrance for the binding of the enzyme to the DNA bearing the TAM label at the 5′ end.

Mutant enzyme APE1N212A cleaves AP-DNA less efficiently than the wild-type enzyme does (Supplementary Figure S1A, lanes 6, 8). The reaction product was absent in the presence of EDTA, which binds the reaction cofactor Mg^{2+} (from $MgCl_2$; Supplementary Figure S1A, lanes 7, 9, 16, 18). Thus, preparation of the DNA/APE1 complex for EPR experiments requires considering possible transformation of the substrate into a product because one has to separate the data on interspin distances for the enzyme–substrate and for the enzyme–product complexes. To prevent conversion of the substrate into the product, we used EDTA in the experiments on APE1 binding to AP-DNA.

Next, we performed a gel shift assay to test the binding efficiency of APE1 to spin-labeled AP-DNA versus control non-spin-labeled substrates. We analyzed the formation of DNA/APE1 complexes by separating this complex (APE1-DNA, Supplementary Figure S2) from free DNA (DNA, Supplementary Figure S2) in non-denaturing PAAG. DNA/APE1 complexes were observed in the gel in the presence of EDTA. The detected binding was not effective, probably because of the modest length of the substrates used in the experiments (12 bp). Nevertheless, to apply PD EPR, we had to use the DNA duplexes of this length, even though the efficiency of interaction with APE1 was lower in this experiment (Supplementary Figure S2). We did not observe the formation of DNA/APE1 complexes in control experiments on DNA without an AP site (Figure 1: *12–3/12–2, *12–3/12–2-TAM, and TAM-12–3/*12–2). The mutant protein APE1N212A showed binding to AP-DNA in both experiments with the control AP-DNA (Supplementary Figure S2A, lanes 3, 7, 8; Supplementary Figure S2B, lane 3) and with the spin-labeled AP-DNA (Supplementary Figure S2A, lanes 12, 13; Supplementary Figure

S2B, lane 6). On the other hand, the data presented in Supplementary Figure S2A indicate that the spin-labeled substrate binds to the protein less efficiently than the control unlabeled AP site containing substrate does (Supplementary Figure S2A, compare lanes 7 and 8 as well as 12 and 13).

Thus, we demonstrated that the spin-labeled AP-DNA duplex is a suitable substrate for the endonuclease reaction catalyzed by APE1. Mutant protein APE1N212A binds to AP-DNA with the same efficiency as the wild-type enzyme does but cleaves AP-DNA less efficiently. Nevertheless, we reached the lowest incision level with rather effective binding after mixing APE1N212A and the spin-labeled AP-DNA for EPR assays. The obtained results display the data on the enzyme–substrate complex formation in the presence of EDTA, but not for the enzyme–product complex.

The spin labels were also introduced into the mutant enzyme (APE1N212A). The spin-labeled protein SL-APE1N212A retains DNA-binding (Supplementary Figure S2B, lanes 4, 7) and endonuclease activity to the same extent as mutant non-spin-labeled protein APE1N212A. Therefore, in our case, introduction of spin labels at the cysteine residues in the protein probably does not create steric hindrance for DNA/protein binding as well as for the catalysis during the endonuclease reaction and thus does not affect the level of enzymatic activity. Hence, we obtained spin-labeled mutant protein SL-APE1N212A, which has the same activity as the initial mutant protein and therefore is suitable for studying the conformation of APE1 in complex with damaged DNA by PD EPR.

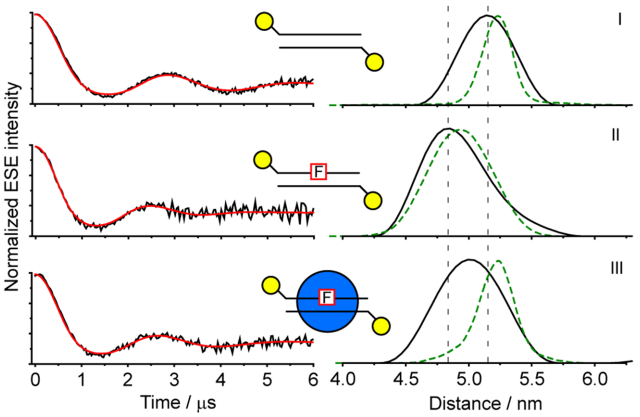

Figure 2. TAM–TAM distance measurements in DNA (I) or DNA with an AP site (II) or AP-DNA in complex with APE1N212A (III) determined by Q-band DQC. (Left) Background-corrected DQC traces (intensity is normalized, line with noise). Solid lines show the best fits obtained using DeerAnalysis2013. (Right) Obtained distance distributions for the studied systems. Regularization parameter L is 100. Dotted lines denote the MD simulations.

Table 1. Mean TAM–TAM distances $\langle r \rangle$ and standard deviations (σ) obtained by DQC and MD simulation

	$<r^{DQC}_{TAM/TAM}> \pm \sigma$ / nm	$<r^{MD}_{TAM/TAM}> \pm \sigma$ / nm
I	5.14 ± 0.20	5.27 ± 0.14
II	4.92 ± 0.27	4.94 ± 0.19
III	5.01 ± 0.24	5.20 ± 0.18

EPR studies of DNA conformations

Prior to studying the AP-DNA/APE1 complexes with both spin-labeled components, we performed auxiliary PD EPR measurements on spin-labeled DNAs and their complexes with unlabeled APE1. We applied the PD EPR method DQC to measure spin–spin distances in a series of DNAs carrying two TAM labels (Figure 2 and Supplementary Figure S5). The series included control DNA (I), DNA with an AP site (AP-DNA, II) and AP-DNA in complex with APE1N212A (III) (Figure 1). The mean distances for the duplex without damage were found to be 5.14 nm (I, Table 1). DQC experiments on two independently prepared samples showed that the experimental error of distance measurements was <0.1 nm. When damage (AP site) was introduced into the DNA, the mean distance decreased to 4.92 nm, being assigned to a change in DNA duplex structure. It is known that the removal of a single nucleobase leads to local structural changes in DNA containing an AP site (16–18). At the same time, it has been shown previously that the TAM label is rigidly localized at the termini of a DNA duplex (54,55). Therefore, we concluded that the observed decrease in the mean distance by 0.2 nm in AP-DNA is related to a change in DNA conformation, not to a change in label conformation. The TAM–TAM distance was found to be 5.01 nm for AP-DNA in complex with APE1N212A (III, Table 1) that was slightly greater as compared to free AP-DNA.

The cleavage of AP-DNA by the wild-type APE1 protein was investigated by PELDOR (Supplementary Figures S7 and S8). For this aim, the distances between two TAMs attached to the ends of AP-DNA were measured in the complex with wild-type APE1 upon the addition of $MgCl_2$. We observed a decrease in the modulation depth versus incubation time of the system at 37°C (2 and 26 h; Supplementary Figure S8B). It should be emphasized that the distribution of interspin distances remained practically unchanged during the conversion of the substrate into the product (Supplementary Figure S8C), and the changes refer only to the decrease in the modulation depth, i.e. in the number of spin pairs (Supplementary Figure S9A), due to the separation of fragments carrying a single label. Hence, we obtained a kinetic curve (Supplementary Figure S9B) and confirmed formation of the DNA product by gel electrophoresis (Supplementary Figure S9C).

To identify the structural changes stemming from the duplex damage and its interaction with the protein, MD simulations of the DNA, AP-DNA and AP-DNA/APE1N212A complexes (I, II and III in Figure 1) were performed. Analysis of the duplex structures revealed that TAMs in these complexes preferentially occupy the positions at duplex termini. Such structural rigidity results in narrow distance distributions observed experimentally. Note that previously, we have found that TAM spin labels do not significantly affect the structure and dynamics of DNA duplexes, and there is a good agreement among distance distributions obtained by EPR, NMR and MD techniques (56,67). In agreement with EPR data, the analysis of MD trajectories of spin-labeled DNA duplexes showed that the AP site (F) leads to a decrease in the distance between two TAM labels [4.94

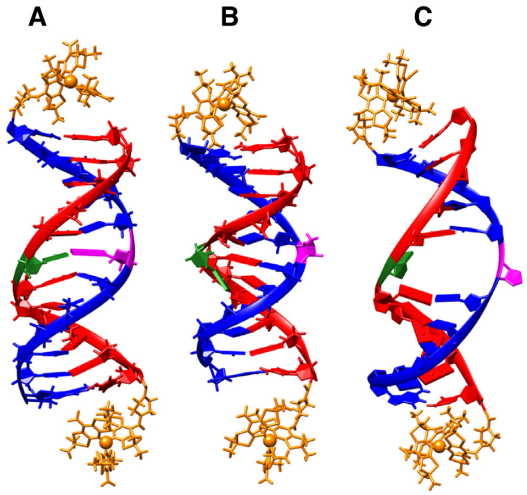

Figure 3. Structures of a double-spin-labeled DNA duplexes obtained by MD simulations: (**A**) undamaged DNA (I), (**B**) DNA with an AP site (AP-DNA, II), (**C**) AP-DNA in complex with APE1N212A (III).

± 0.19 nm for AP-DNA (II) versus 5.27 ± 0.14 nm for control DNA (I), Table 1]. This decrease can be explained by displacement of the unpaired cytidine opposite the AP site; this change leads to stacking of the nearest base pairs surrounding the damaged site (Figure 3B). According to the literature, the scale of the structural changes in AP-DNA depends on the nucleotide context at the damaged site, e.g. in the case of cytosine opposite an AP site, the double helix could collapse (18). For complex II, the cytidine residue does not engage in efficient stacking with the surrounding base pairs and thus can be displaced to the major groove, whereas the nucleotide pairs near the damaged site manifest efficient stacking, which stabilizes the duplex. Ultimately, this reduces the length of the double helix and its torsion at the damaged site, and provokes slight bending (Figure 3) (18). The distance distributions obtained by MD simulations are in good agreement with those obtained by EPR (Figure 2 and Table 1).

Analysis of the AP-DNA structure in the complex with APE1N212A indicates the stretching of DNA mainly at the damaged site and in the nearest regions, which is caused by coordination of the ribose-phosphate backbone by amino acid residues (Figure 3C). These structural rearrangements of AP-DNA upon formation of a complex with APE1 have been previously found experimentally by X-ray crystallography (35,68,69) and theoretically by MD simulations (70) and are very close to the structural rearrangements observed by us.

EPR studies of spin-labeled mutant APE1 (APE1N212A)

The last step before PD EPR studies of AP-DNA/APE1 complexes is the examination of spin-labeled mutant APE1. CW EPR was applied to control and confirm the nitroxide labeling of APE1N212A. Experimental EPR spectra and simulations are shown in Supplementary Figures S3 and S4. The spin-labeling efficiency estimated from the CW EPR data was two spins per one APE1N212A molecule. Spectrum modeling allowed us to estimate that roughly 60–70% of labels were attached to a protein and underwent slow anisotropic rotation (broad lines; orientation potential needs to be included) (Supplementary Table S1). Then, 20–30% of labels are also attached to a protein, but manifest faster anisotropic motion (orientation potential is also necessary); therefore, they are most likely attached at a different position. Finally, 5–10% of labels corresponded to an admixture of free nitroxides. Fitting of the X-band CW EPR spectrum of a nitroxide with such a large number of components does not lead to a unique solution; accordingly, the ratio of the fractions cannot be determined precisely.

Analysis of mass-spectrometric data after trypsin digestion of the spin-labeled protein indicates attachment of nitroxide spin labels at three positions (Figure 4B): Cys138 (N1), Cys296 (N3) and Cys310 (N2). MD simulations revealed that the conformational mobility of the nitroxide labels attached to APE1N212A differs among the three residues. The spin label (N1) attached to Cys138 is located on the external surface of the protein and can move freely around the attachment site with only slight steric hindrance from the protein side. The N2 spin label attached to Cys310 is located inside the protein; therefore, its mobility is strongly restricted. The third label (N3; attached to Cys296) denotes an intermediate case: there is some degree of freedom, but the localization between the protein core and Asp50-Ala60–loop introduces significant steric restrictions (Figure 4B). These structural features were found by the analysis of MD trajectories: the root mean square deviation (RMSD) values for the nitroxide residues were 2.7, 1.7 and 0.3 Å for N1, N2 and N3, respectively. Consequently, the mobility of two spin labels out of the three is restricted, in good agreement with the CW EPR data.

PELDOR experiments on SL-APE1N212A reveal a detectable dipolar oscillation (Figure 4A). Analysis of PELDOR data in DeerAnalysis 2013 (63) yielded a multimodal distance distribution between nitroxides in the range of 1 to 6 nm with a major peak at 2.4 nm. The observed modulation depth (9.5%) is higher than the maximal one (6.5%) anticipated for two coupled nitroxides in our experimental setup and settings (see 'Materials and Methods' section). The number of radicals contributing to the PELDOR signal, $N \approx 2.6$, was estimated via the equation $N = 1 + \ln(V_\infty)/\ln(1 - \lambda_B)$ (71,72). Because CW EPR data indicate that each APE1N212A molecule contains only two spin labels, the PELDOR findings should be interpreted as superposition of signals from monomers and dimers. The formation of APE1 dimers has previously been detected by dynamic light scattering (73,74). Thus, in the absence of a DNA substrate, APE1 molecules can form homodimers that are detectable by EPR. Next, we conducted PELDOR experiments on the complex of spin-labeled protein SL-APE1N212A with AP-DNA. Evidently, the addition of AP-DNA to SL-APE1N212A affects both modulation depth and distance distribution, and the same was found to be true for TAM-labeled AP-DNA (complex V in Figure 4 and Supplementary Figure S10). The modulation depth (~7%) for SL-APE1N212A in complex with AP-DNA corresponds well to the two coupled nitroxides and points to the absence of a dimeric form of the APE1N212A/AP-DNA complex. Therefore, in this case

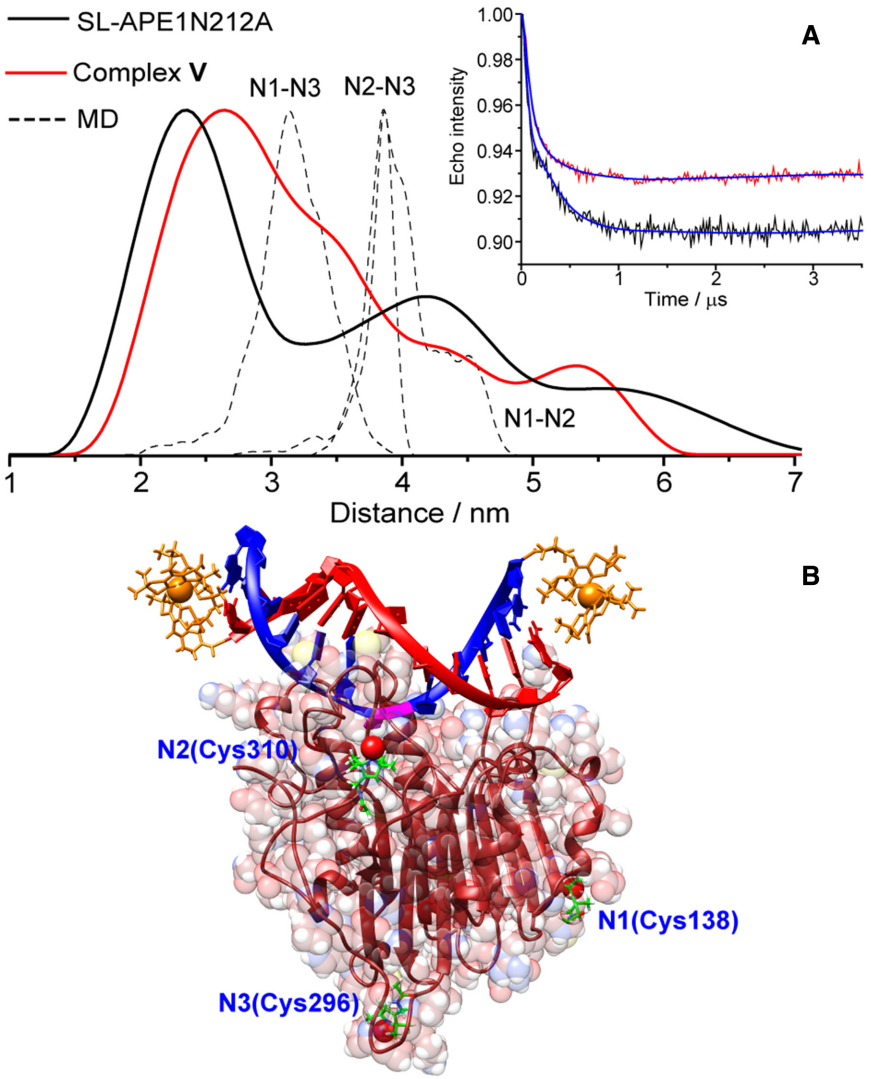

Figure 4. (**A**) Distance distribution between nitroxide spin labels in APE1N212A: dotted lines results of MD calculation, solid lines experimental data obtained by PELDOR. The inset shows a normalized PELDOR time trace at 50 K and simulation using DeerAnalysis. (**B**) The calculated structure of the AP-DNA/APE1N212A complex.

PELDOR data should be interpreted as the pairwise distribution inside one protein molecule.

We analyzed distances within all three possible pairs of the nitroxide labels at equilibrium MD trajectories of the complex in an explicit water shell. Calculated interspin distance distributions for each pair are illustrated in Figure 4A; their superposition falls into the range of 2 to 5 nm. The distance distribution determined by EPR is broader and spreads over the range of 1.5 to 6.0 nm. The imperfect agreement between MD and EPR distances is possibly due to the limitations of the calculation method employed for this large system, in particular insufficient structure sampling of the spin-labeled protein. Nevertheless, rather reasonable qualitative agreement can be achieved. The shortest calculated interspin distance was obtained for the N1–N3 pair, and therefore the major peak at 2.6 nm in the experimentally obtained distribution was assigned to the distance in this pair (Figure 4A). This assignment is rather reasonable because Cys138 (N1) and Cys296 (N3) are situated on the external surface of the protein globule and potentially are more available for spin labeling, whereas Cys310 (N2) is shielded by surrounding β-sheets of the protein and is less accessible for spin labeling (Figure 4B).

Studies of the AP-DNA/APE1N212A complex labeled orthogonally

Finally, we applied PD EPR to study the AP-DNA/APE1 complexes of spin-labeled protein and spin-labeled DNA. The use of two or more different (orthogonal) spin labels has significant advantages over the use of labels of the same type (58,75,76). This notion becomes especially evident when complicated systems with more than two spin labels are studied. In this work, we performed PELDOR experiments on DNA/protein complexes labeled orthogonally, where nitroxides were introduced into APE1N212A, and a single TAM label was attached to one of DNA ends

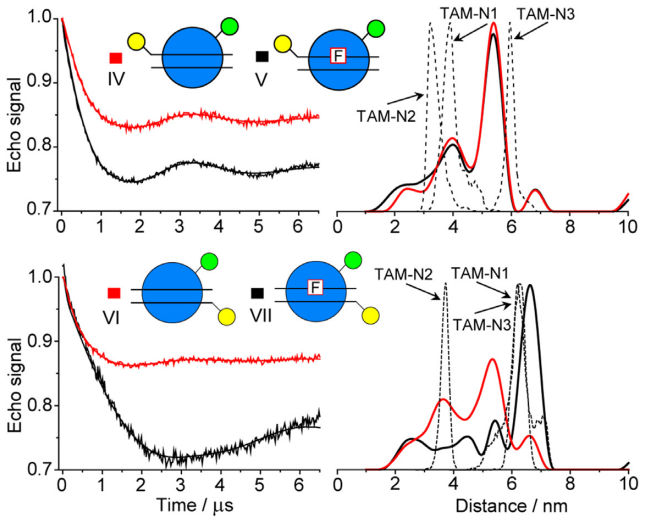

Figure 5. Distance measurements in the mixtures of nitroxide-labeled APE1N212A and single-TAM-labeled DNA or AP-DNA obtained by Q-band PELDOR. (Left) Background-corrected PELDOR traces (intensity is normalized). Lines with noise correspond to the experimental data. Solid lines show the best fits obtained using DeerAnalysis 2013. (Right) The obtained distance distributions for the systems under study. Regularization parameter *L* is 1000. Dotted lines show the MD simulations for the complex of TAM-labeled AP-DNA and nitroxide-labeled APE1N212A (IV–VII).

(complexes IV–VII in Figure 1). We chose the main EPR line of TAM for pumping and the nitroxide signal for observing (Supplementary Figure S6).

The obtained PELDOR data allowed us to analyze the formation of complexes of APE1N212A with native or damaged DNA. Dipolar oscillations were detected for all four complexes IV–VII (Figure 5). The modulation depth (23.5% and 25.5%) in the complexes with AP-DNA (V and VII) matches well the expected one (24%) for the nitroxide–TAM pair (see the 'Materials and Methods' section), suggesting that most of AP-DNA and APE1N212A form a complex at the used concentrations. For undamaged DNA, we also detected formation of the complex with APE1N212A (complexes V and VII), and the modulation depth in this case was only 2-fold smaller than that in the complex with damaged DNA.

The observed distance distributions between the TAM label attached at the 5′ end of the 'damaged' strand (IV, V) and the nitroxide labels within the protein were found to be the same for the complexes with and without damage (the major peak at 5.5 nm). When the TAM label was attached at the 5′ end of the undamaged complementary strand (VI, VII), the distance distributions turned out to be significantly different. Both complexes underwent changes in the range of 2 to 6 nm, and in addition, the APE1N212A complex with AP-DNA featured a large peak with a maximum at 6.5 nm (Figure 5).

We performed MD simulations of the structures of AP-DNA/APE1N212A complexes (V and VII) and analyzed TAM–nitroxide distances for three possible attachment sites of the nitroxide. MD-based distance distribution reproduces the trends observed experimentally in PELDOR data for both complexes (black solid and dashed lines in Figure 5). The highest peak at the ∼5.4 nm in the experimental distribution for complex V is close to the TAM–N3 distance of 5.9 nm calculated via MD simulation. Additional peaks in the range 2–5 nm were determined by MD simulation and correspond to the distances between TAM and N1 or N2. In case of complex VII, MD simulation yielded similar distances of ∼6.3 nm between TAM and two of three nitroxides (N1 and N3) and is well consistent with PELDOR data displaying a dominant peak at 6.6 nm. The comparison of calculated and experimental distance distributions suggests that the nitroxide-labeling efficiencies in positions N3 and N1 are higher than that at position N2. This finding is in good agreement with the analysis of the distance distribution between nitroxides in SL-APE1N212A. Note that MD simulations could not be performed on the complex of APE1N212A with undamaged DNA because in this case, the protein does not specifically interact with the duplex.

DISCUSSION

APE1 is the main AP endonuclease in mammalian cells and plays a major role in the DNA base excision repair (BER) system initiating the removal of AP sites. APE1 has additional activities aimed at preserving the integrity of the genome (77,78). The numerous functions of APE1 attract the attention of researchers, and therefore this enzyme is studied actively. Several research groups have reported structural studies on this enzyme and on DNA/APE1 complexes by various methods, including X-ray analysis. Nonetheless, these structural data on DNA/APE1 complexes are rather divergent; therefore, it is necessary to develop additional methods for structural investigation of DNA/APE1 complexes. In this work, we for the first time employed PD EPR and TAM spin labeling of a DNA duplex in conjunction with nitroxide labeling of APE1. The EPR experiments were combined with MD simulations to investigate the conformational changes occurring in AP-DNA and in the DNA/APE1 complex.

We demonstrated that a TAM-labeled AP-DNA duplex is a suitable substrate for studying the endonuclease reaction catalyzed by wild-type APE1 or by a mutant enzyme. The APE1 mutant with the N212A substitution has a lower AP endonuclease activity but binds to a damaged DNA with the same efficiency as does the wild-type enzyme (Supplementary Figure S2). Therefore, this APE1 mutant can be used to analyze the AP-DNA/APE1 complex formation in the absence of Mg^{2+}. Consequently, this experimental model is close to a 'catalytically competent' complex of APE1 with AP-DNA.

It is known that the presence of an AP site in DNA influences the structure and flexibility of the DNA helix, which is important for recognition of the damage during repair (22,23). The sequence of the opposite strand of AP-DNA is also important because natural nucleotides affect the DNA helix structure at a damage site differently. This may affect the DNA/APE1 complex formation and the efficiency of the endonuclease reaction. NMR studies have shown that dAMP (deoxyadenosine monophosphate) opposite the AP site does not distort the helix compared to intact DNA, whereas dCMP (deoxycytidine monophos-

phate) and dGMP (deoxyguanosine monophosphate) cause a change in the helix structure to varying degrees, resulting in flipping of a nucleotide and/or the AP site (79). We determined the distance distribution and mean distances between two TAM spin labels at the 5′ ends of DNA duplexes via EPR and MD simulations. The intact DNA and AP site (F, opposite dCMP)-containing DNA were subjected to the experiments. It was revealed that introduction of a model AP site leads to a slight decrease in the mean distance between the two TAM spin labels (Table 1).

EPR was recently applied to the investigation of conformational changes in a DNA duplex containing different types of damage (19). It was found that the introduction of F leads to a slight decrease of the distance between two nitroxide spin labels (4-amino-TEMPO). The authors (20) have noted that this decrease may be attributed to DNA's bending around the inserted AP site at an angle of 20°. The distance distribution between nitroxide spin labels in the damaged DNA duplex observed in that work was broad and contained several maxima. Application of TAM labels in the present study allowed us to obtain narrower distance distributions owing to the advantageous properties of TAMs.

The biochemical experiments indicate that changes in the structure and flexibility of DNA may influence the ability of proteins to recognize the damage. Among pairs with a normal base located opposite F (F/A, C, G, T), APE1 cleaves the AP site nearly with the same efficiency (30). When a damaged base (dihydrothymidine or 8-oxoguanine) is located opposite F or at a distance of three or five nucleotides from the 3′ or 5′ side of the AP site, the efficiency of APE1 cleavage is almost unchanged (80). The introduction of an AP site opposite another AP site (30) or at one or three nucleotides on the 3′ side of the AP site (80) results in significant inhibition of the endonuclease activity of APE1. The latter activity is significantly suppressed when there is a noncanonical pair on the 5′ side of the F residue. On the contrary, the presence of a noncanonical pair on the 3′ side practically does not affect the efficiency of this reaction (30). The analysis of crystal structures of APE1 (32–34) and DNA/APE1 complexes (35–37) has uncovered the bending of the DNA helix and extrahelical flipping of F (35,38). It should be noted that X-ray analysis detects only one most stable conformation of a DNA/protein complex: the one that crystallizes; but such a conformation does not necessarily correspond to the conformation of the complex in solution. It is quite possible that for some reason, the conformation of a protein that matches the true location of the DNA duplex is not the one visible in X-ray analysis.

In publication (19) the authors have stated that APE1 induces significant additional bending of DNA with different types of damage, including F. They concluded that APE1 attempts to bend DNA until the damaged nucleotide flips out of the double helix into the active site of the enzyme. It should be noted that those authors did not measure the mean distance for AP-DNA in the DNA/APE1 complex by PELDOR; they only evaluated it by MD analysis. The broad distribution obtained in PELDOR and the quite narrow one seen in MD simulation allowed the authors (19) to compare their data only qualitatively. When nitroxide labels are attached to relatively short DNA duplexes, these labels are typically located far away from the helix axis because of their high mobility. In particular, this occurs because the duplex width (∼2 nm) becomes comparable with its length (3.4 nm for 10 bp). In case of TAM labels, the observed distances can be more reliably attributed to the bending of the double helix because spin centers are located near the duplex axis (Supplementary Figure S12). As we have reported previously (47), the distance distribution observed for a DNA duplex double-labeled with nitroxides is substantially broader than that in a double-TAM-labeled duplex. This finding was explained by the hydrophobicity of TAM leading to its preferred localization at the duplex termini, whereas the nitroxide label does not engage in these specific interactions and can move freely. This is an important advantage of TAM spin labels. Our EPR experiments suggest that the mean TAM–TAM distance for AP-DNA slightly increases after AP-DNA/APE1 complex formation (Table 1). The MD analysis indicates that in the complex with the protein, the DNA duplex becomes more expanded and less helical, and the AP site is flipped out from the DNA helix and located in the protein catalytic pocket.

The observed change in the distance between nitroxide labels attached to DNA has previously been ascribed solely to the duplex bending (19). Nevertheless, the effects that may induce such changes in damaged DNA include (i) bending of the duplex owing to the damage; (ii) relative twisting of two flanking fragments of AP-DNA (rotation of one fragment relative to the other); (iii) a decrease in the distances between neighboring base pairs of the abasic site because of the stacking. Other important parameters that affect the observed interspin distance are the length of the linker between the spin label and oligonucleotide and the properties (hydrophobic or hydrophilic) of the label. Supplementary Figure S12 sketches the effects of linker length and label types (nitroxide versus TAM) on the interspin distance for a native and damaged DNA duplex.

Shortening of the distances between base pairs next to the abasic site (on either side) owing to the stacking is the most crucial aspect for studied DNA duplex. In case of the F-containing DNA (II, Table1), we observed that the cytosine opposite the damage site is flipped out, as is the AP site itself; this situation leads to the 'collapse' of the base pairs adjacent to the damage site.

As shown previously, the above effect of stacking is strongly dependent on the nature of base pairs adjacent to the damage site (18). For instance, in case of sequence CXC (X denotes any nucleotide), unpaired purines at the X position are found to lie within the helix, whereas unpaired pyrimidines are either extrahelical or in the equilibrium between the intra- and extrahelical forms (18). For the GXG fragment, all unpaired bases X lead to intrahelical forms, but sequence-dependent differences in the induced curvature were noted. The observed sequence dependence of the 'collapse' in the central part of the duplex originates from the weak stacking of the X base with the neighboring base pairs. A similar observation was made in the studied duplex with an AP site opposite the cytosine in the GCG site. Thus, shortening of the distance between two TAM residues is mainly determined by the 'collapse' of the central part of the duplex, not by the bending of the helix.

The structure of the spin-labeled protein in the complex with AP-DNA obtained by MD simulation (most represented in the trajectories generated by cluster analysis) is well consistent with the X-ray structures (PDBID: 1de8, 1dew, 5cfg, 5dff, 5dfi, 5wn0, 5wn2, and 5wn4). RMSD values between the calculated and experimental structures for the C_α carbons of the protein are <1 Å. Several existing experimental X-ray structures of APE1 are extremely close: RMSD for C_α carbons of the protein is <0.4 Å. MD-calculated structures of DNA duplexes in the DNA/APE1 complex did not match the experimental X-ray structures so well (Supplementary Figure S11). The central fragment of the duplex perfectly matches the experiment, but there is turnover on the right side of the duplex (Supplementary Figure S11). This difference could originate from the nucleotide sequence, the presence of a massive charged spin label, or force field inaccuracy.

It is known that the affinity of APE1 is higher for a damaged DNA containing an AP site than for intact DNA because of the strong specificity of APE1 to AP sites (81–83). The binding efficiency of APE1 for a DNA substrate with an AP site is at least an order of magnitude higher than that for an incised DNA product (83,84). Our EPR data revealed that the modulation depth in PELDOR correlates with binding efficiency and can be used to evaluate the binding of APE1 with intact or damaged DNA. This approach indicates a stronger binding for a damaged DNA; this finding is consistent with the data obtained by the gel-shift assay for our DNA structures. A possible reason why the authors of (19) did not measure the distance by PELDOR for AP-DNA is the strong enzymatic activity of APE1, which hydrolyzes DNA at a high reaction rate. We managed to slow down APE1 activity by adding EDTA and then started the reaction by adding an excess of magnesium chloride. This method allowed us to follow the dynamics of the PELDOR signal during the DNA substrate-to-product transformation (Supplementary Figure S9). Thus, our complex PD EPR study allows successful monitoring of AP-DNA cleavage by APE1.

CONCLUSION

In this article, we investigated DNA containing an AP site (F damage) as well as complexes of DNA with APE1 by PD EPR distance measurements and MD calculations. F is often utilized as a model of an enzymatically generated AP site, and the complexes we researched are the most important models for identifying the mechanism of DNA repair. Implementation of nitroxide spin labeling of APE1 in combination with TAM spin labeling of DNA allowed us to perform PELDOR on orthogonal spin labels confirm the formation of a DNA/APE1 complex, and explore the structural aspects of protein–nucleic acid systems.

We have demonstrated for the first time that modulation depth in the PELDOR of this system can be used for evaluation of the binding of APE1 to a DNA duplex containing an AP site as well as to monitor the DNA cleavage by APE1. Moreover, we have demonstrated that TAM spin labels attached at DNA termini have substantial advantages compared to previous applications of nitroxides. First, TAM labels allow for more precise distance measurements because they yield narrower distance distributions due to their interactions with DNA duplex ends. Second, for the same reason, these distances can be more reliably translated into structural information because the fixation of TAMs at the duplex termini has been established experimentally and theoretically in a series of other works (54,56,67). Finally, for the specific task of the present study, such a location of TAMs (capping the duplex) yields superior sensitivity to the bending effects in a DNA duplex containing an AP site and in the DNA/APE1 complex.

Indeed, the dynamic structure of the damaged DNA complex with APE1N212A determined from EPR and MD data is in good agreement with the X-ray structure and shows that (i) the DNA helix is bent, and (ii) F is flipped out of the helix into a specific binding pocket of the protein. By EPR spectroscopy, we detected the formation of APE1 homodimers in the absence of DNA but did not obtain the evidence of a dimeric form of the DNA/APE1 complex.

In summary, in this study, we developed and applied a new approach to DNA/protein complexes investigation using orthogonal spin-labeling with TAMs and nitroxides and PD EPR. This approach is broadly applicable but was found to be especially useful to study DNA complexes with APE1. Given that APE1 is broadly involved in various key processes in the cell and in interactions with numerous proteins, the obtained spin-labeled form of APE1 is a highly promising tool for analysis of protein–protein interactions of this enzyme in DNA repair, replication, and transcription processes.

SUPPLEMENTARY DATA

Supplementary Data are available at NAR Online.

ACKNOWLEDGEMENTS

We thank Dr. Vladimir A. Richter, Dr. Anna V. Savelyeva and Dr. Alexander S. Fomin for their help with production and purification of mutant APE1 protein. We also thank Marat F. Kasakin for his help with MALDI analysis and identification of spin-labeling sites within the APE1 protein.

FUNDING

Ministry of Science and Education of the Russian Federation [14.W03.31.0034]; Russian Science Foundation [14–14–00922]. Funding for open access charge: Ministry of Science and High Education of Russian Federation [14.W03.31.0034].
Conflict of interest statement. Olesya A. Krumkacheva, Nadezhda S. Dyrkheeva, Georgiy Shevelev and Alexander Lomzov contributed qually.

REFERENCES

1. Lindahl,T. (1993) Instability and decay of the primary structure of DNA. *Nature*, **362**, 709–715.
2. Krokan,H.E., Standal,R. and Slupphaug,G. (1997) DNA glycosylases in the base excision repair of DNA. *Biochem. J.*, **325**, 1–16.
3. Lindahl,T. (1980) [36]Uracil-DNA glycosylase from Escherichia coli. *Methods Enzymol.*, **65**, 284–290.

4. Nash,H.M., Bruner,S.D., Schärer,O.D., Kawate,T., Addona,T.A., Spooner,E., Lane,W.S. and Verdine,G.L. (1996) Cloning of a yeast 8-oxoguanine DNA glycosylase reveals the existence of a base-excision DNA-repair protein superfamily. *Curr. Biol.*, **6**, 968–980.
5. Dizdaroglu,M., Karahalil,B., Sentürker,S., Buckley,T.J. and Roldán-Arjona,T. (1999) Excision of products of oxidative DNA base damage by human NTH1 protein. *Biochemistry*, **38**, 243–246.
6. Wyatt,M.D., Allan,J.M., Lau,A.Y., Ellenberger,T.E. and Samson,L.D. (1999) 3-methyladenine DNA glycosylases: structure, function, and biological importance. *BioEssays*, **21**, 668–676.
7. Loeb,L.A. and Preston,B.D. (2003) Mutagenesis by apurinic/apyrimidinic sites. *Annu. Rev. Genet.*, **20**, 201–230.
8. Boiteux,S. and Laval,J. (1982) Coding properties of poly(deoxycytidylic acid) templates containing uracil or apyrimidinic sites: in vitro modulation of mutagenesis by deoxyribonucleic acid repair enzymes. *Biochemistry*, **21**, 6746–6751.
9. Sagher,D. and Strauss,B. (1983) Insertion of nucleotides opposite apurinic apyrimidinic sites in deoxyribonucleic acid during in vitro synthesis: uniqueness of adenine nucleotides. *Biochemistry*, **22**, 4518–4526.
10. Randall,S.K., Eritja,R., Kaplan,B.E., Petruska,J. and Goodman,M.F. (1987) Nucleotide insertion kinetics opposite abasic lesions in DNA. *J. Biol. Chem.*, **262**, 6864–6870.
11. Kokoska,R.J., Bebenek,K., Boudsocq,F., Woodgate,R. and Kunkel,T.A. (2002) Low fidelity DNA synthesis by a y family DNA polymerase due to misalignment in the active site. *J. Biol. Chem.*, **277**, 19633–19638.
12. Kokoska,R.J., McCulloch,S.D. and Kunkel,T.A. (2003) The efficiency and specificity of apurinic/apyrimidinic site bypass by human DNA polymerase η and sulfolobus solfataricus Dpo4. *J. Biol. Chem.*, **278**, 50537–50545.
13. Cuniasse,P., Fazakerley,G.V., Guschlbauer,W., Kaplan,B.E. and Sowers,L.C. (1990) The abasic site as a challenge to DNA polymerase. *J. Mol. Biol.*, **213**, 303–314.
14. Marathias,V.M., Jerkovic,B. and Bolton,P.H. (1999) Damage increases the flexibility of duplex DNA. *Nucleic Acids Res.*, **27**, 1854–1858.
15. Hoehn,S.T., Turner,C.J. and Stubbe,J. (2001) Solution structure of an oligonucleotide containing an abasic site: evidence for an unusual deoxyribose conformation. *Nucleic Acids Res.*, **29**, 3413–3423.
16. Chen,J., Dupradeau,F.-Y., Case,D.A., Turner,C.J. and Stubbe,J. (2008) DNA oligonucleotides with A, T, G or C opposite an abasic site: structure and dynamics. *Nucleic Acids Res.*, **36**, 253–262.
17. Osakabe,A., Arimura,Y., Matsumoto,S., Horikoshi,N., Sugasawa,K. and Kurumizaka,H. (2017) Polymorphism of apyrimidinic DNA structures in the nucleosome. *Sci. Rep.*, **7**, 41783.
18. Ayadi,L., Coulombeau,C. and Lavery,R. (1999) Abasic sites in duplex DNA: molecular modeling of sequence-dependent effects on conformation. *Biophys. J.*, **77**, 3218–3226.
19. Kuznetsova,A.A., Matveeva,A.G., Milov,A.D., Vorobjev,Y.N., Dzuba,S.A., Fedorova,O.S. and Kuznetsov,N.A. (2018) Substrate specificity of human apurinic/apyrimidinic endonuclease APE1 in the nucleotide incision repair pathway. *Nucleic Acids Res.*, **46**, 11454–11465.
20. Kuznetsov,N.A., Milov,A.D., Koval,V. V., Samoilova,R.I., Grishin,Y.A., Knorre,D.G., Tsvetkov,Y.D., Fedorova,O.S. and Dzuba,S.A. (2009) PELDOR study of conformations of double-spin-labeled single- and double-stranded DNA with non-nucleotide inserts. *Phys. Chem. Chem. Phys.*, **11**, 6826–6832.
21. Isaev,N.P., Tsvetkov,Y.D., Dzuba,S.A., Milov,A.D., Vorobjev,Y.N., Fedorova,O.S., Kuznetsov,N.A. and Koval,V.V. (2011) PELDOR analysis of enzyme-induced structural changes in damaged DNA duplexes. *Mol. BioSyst.*, **7**, 2670.
22. Jen-Jacobson,L., Engler,L.E. and Jacobson,L.A. (2000) Structural and thermodynamic strategies for site-specific DNA binding proteins. *Structure*, **8**, 1015–1023.
23. Yang,W. (2008) Structure and mechanism for DNA lesion recognition. *Cell Res.*, **18**, 184–197.
24. Xu,Y.J., Kim,E.Y. and Demple,B. (1998) Excision of C-4′-oxidized deoxyribose lesions from double-stranded DNA by human apurinic/apyrimidinic endonuclease (Ape1 protein) and DNA polymerase beta. *J. Biol. Chem.*, **273**, 28837–28844.
25. Masuda,Y., Bennett,R.A. and Demple,B. (1998) Dynamics of the interaction of human apurinic endonuclease (Ape1) with its substrate and product. *J. Biol. Chem.*, **273**, 30352–30359.
26. Maher,R.L. and Bloom,L.B. (2007) Pre-steady-state kinetic characterization of the AP endonuclease activity of human AP endonuclease 1. *J. Biol. Chem.*, **282**, 30577–30585.
27. Schermerhorn,K.M. and Delaney,S. (2013) Transient-state kinetics of apurinic/apyrimidinic (AP) endonuclease 1 acting on an authentic AP Site and commonly used substrate analogs: the effect of diverse metal ions and base mismatches. *Biochemistry*, **52**, 7669–7677.
28. Erzberger,J.P. and Wilson,D.M. (1999) The role of Mg2+ and specific amino acid residues in the catalytic reaction of the major human abasic endonuclease: new insights from EDTA-resistant incision of acyclic abasic site analogs and site-directed mutagenesis. *J. Mol. Biol.*, **290**, 447–457.
29. Kutuzov,M.M., Ilina,E.S., Sukhanova,M.V., Pyshnaya,I.A., Pyshnyi,D.V., Lavrik,O.I. and Khodyreva,S.N. (2011) Interaction of poly(ADP-ribose) polymerase 1 with apurinic/apyrimidinic sites within clustered DNA damage. *Biochem.*, **76**, 147–156.
30. Wilson,D.M., Takeshita,M., Grollman,A.P. and Demple,B. (1995) Incision activity of human apurinic endonuclease (Ape) at abasic site analogs in DNA. *J. Biol. Chem.*, **270**, 16002–16007.
31. Kanazhevskaya,L.Y., Koval,V.V., Vorobjev,Y.N. and Fedorova,O.S. (2012) Conformational dynamics of abasic DNA upon interactions with AP endonuclease 1 revealed by stopped-flow fluorescence analysis. *Biochemistry*, **51**, 1306–1321.
32. Manvilla,B.A., Pozharski,E., Toth,E.A. and Drohat,A.C. (2013) Structure of human apurinic/apyrimidinic endonuclease 1 with the essential Mg2+ cofactor. *Acta Crystallogr. D. Biol. Crystallogr.*, **69**, 2555–2562.
33. Beernink,P.T., Segelke,B.W., Hadi,M.Z., Erzberger,J.P., Wilson,D.M. and Rupp,B. (2001) Two divalent metal ions in the active site of a new crystal form of human apurinic/apyrimidinic endonuclease, ape1: implications for the catalytic mechanism 1 1Edited by I. A. Wilson. *J. Mol. Biol.*, **307**, 1023–1034.
34. Gorman,M.A., Morera,S., Rothwell,D.G., de La Fortelle,E., Mol,C.D., Tainer,J.A., Hickson,I.D. and Freemont,P.S. (1997) The crystal structure of the human DNA repair endonuclease HAP1 suggests the recognition of extra-helical deoxyribose at DNA abasic sites. *EMBO J.*, **16**, 6548–6558.
35. Mol,C.D., Izumi,T., Mitra,S. and Tainer,J.A. (2000) DNA-bound structures and mutants reveal abasic DNA binding by APE1 DNA repair and coordination. *Nature*, **403**, 451–456.
36. Mol,C.D., Hosfield,D.J. and Tainer,J.A. (2000) Abasic site recognition by two apurinic/apyrimidinic endonuclease families in DNA base excision repair: the 3′ ends justify the means. *Mutat. Res.*, **460**, 211–229.
37. Tsutakawa,S.E., Shin,D.S., Mol,C.D., Izumi,T., Arvai,A.S., Mantha,A.K., Szczesny,B., Ivanov,I.N., Hosfield,D.J., Maiti,B. *et al.* (2013) Conserved structural chemistry for incision activity in structurally non-homologous apurinic/apyrimidinic endonuclease APE1 and endonuclease IV DNA repair enzymes. *J. Biol. Chem.*, **288**, 8445–8455.
38. Hosfield,D.J., Guan,Y., Haas,B.J., Cunningham,R.P. and Tainer,J.A. (1999) Structure of the DNA repair enzyme endonuclease IV and its DNA complex: double-nucleotide flipping at abasic sites and three-metal-ion catalysis. *Cell*, **98**, 397–408.
39. Carey,D.C. and Strauss,P.R. (1999) Human apurinic/apyrimidinic endonuclease is processive. *Biochemistry*, **38**, 16553–16560.
40. Schiemann,O. and Prisner,T.F. (2007) Long-range distance determinations in biomacromolecules by EPR spectroscopy. *Q. Rev. Biophys.*, **40**, 1–53.
41. Jeschke,G. and Polyhach,Y. (2007) Distance measurements on spin-labelled biomacromolecules by pulsed electron paramagnetic resonance. *Phys. Chem. Chem. Phys.*, **9**, 1895–1910.
42. Duss,O., Yulikov,M., Jeschke,G. and Allain,F.H.T. (2014) EPR-aided approach for solution structure determination of large RNAs or protein-RNA complexes. *Nat. Commun.*, **5**, 3669–3678.
43. Borbat,P.P. and Freed,J.H. (2013) Pulse dipolar electron spin resonance: Distance measurements. In: Timmel,CR and Harmer,JR (eds). *Structure and Bonding*. Springer-Verlag, Berlin Heidelberg, Vol. **152**, pp. 1–82.
44. Milov,A.D., Salikhov,K.M. and Shchirov,M.D. (1981) Use of the double resonance in electron spin echo method for the study of

paramagnetic center spatial distribution in solids. *Fiz. Tverd. Tela*, **23**, 975–982.
45. Borbat,P.P. and Freed,J.H. (1999) Multiple-quantum ESR and distance measurements. *Chem. Phys. Lett.*, **313**, 145–154.
46. Prisner,T.F., Marko,A. and Sigurdsson,S.T. (2015) Conformational dynamics of nucleic acid molecules studied by PELDOR spectroscopy with rigid spin labels. *J. Magn. Reson.*, **252**, 187–198.
47. Stelzl,L.S., Erlenbach,N., Heinz,M., Prisner,T.F. and Hummer,G. (2017) Resolving the conformational dynamics of DNA with angstrom resolution by pulsed electron–electron double resonance and molecular dynamics. *J. Am. Chem. Soc.*, **139**, 11674–11677.
48. Reginsson,G.W., Shelke,S.A., Rouillon,C., White,M.F., Sigurdsson,S.T. and Schiemann,O. (2012) Protein-induced changes in DNA structure and dynamics observed with noncovalent site-directed spin labeling and PELDOR. *Nucleic Acids Res.*, **41**, e11.
49. Babaylova,E.S., Malygin,A.A., Lomzov,A.A., Pyshnyi,D.V., Yulikov,M., Jeschke,G., Krumkacheva,O.A., Fedin,M.V., Karpova,G.G. and Bagryanskaya,E.G. (2016) Complementary-addressed site-directed spin labeling of long natural RNAs. *Nucleic Acids Res.*, **44**, 7935–7943.
50. Malygin,A.A., Graifer,D.M., Meschaninova,M.I., Venyaminova,A.G., Timofeev,I.O., Kuzhelev,A.A., Krumkacheva,O.A., Fedin,M.V., Karpova,G.G. and Bagryanskaya,E.G. (2018) Structural rearrangements in mRNA upon its binding to human 80S ribosomes revealed by EPR spectroscopy. *Nucleic Acids Res.*, **46**, 897–904.
51. Krumkacheva,O. and Bagryanskaya,E. (2017) Trityl radicals as spin labels. In: *Electron Paramagnetic Resonance*. The Royal Society of Chemistry, London, Vol. **25**, pp. 35–60.
52. Borbat,P., Freed,J.H., Liu,Y., Zweier,J.L., Hubbell,W.L. and Yang,Z. (2012) Pulsed ESR dipolar spectroscopy for distance measurements in immobilized spin labeled proteins in liquid solution. *J. Am. Chem. Soc.*, **134**, 9950–9952.
53. Reginsson,G.W., Kunjir,N.C., Sigurdsson,S.T. and Schiemann,O. (2012) Trityl radicals: spin labels for nanometer-distance measurements. *Chem. Eur. J.*, **18**, 13580–13584.
54. Shevelev,G.Y., Krumkacheva,O.A., Lomzov,A.A., Kuzhelev,A.A., Trukhin,D.V., Rogozhnikova,O.Y., Tormyshev,V.M., Pyshnyi,D.V., Fedin,M.V. and Bagryanskaya,E.G. (2015) Triarylmethyl labels: toward improving the accuracy of EPR nanoscale distance measurements in DNAs. *J. Phys. Chem. B*, **119**, 13641–13648.
55. Tormyshev,V.M., Bagryanskaya,E.G., Fedin,M.V., Yulikov,M., Shevelev,G.Y., Pyshnyi,D.V. and Jeschke,G. (2016) Interaction of triarylmethyl radicals with DNA termini revealed by orientation-selective W-band double electron–electron resonance spectroscopy. *Phys. Chem. Chem. Phys.*, **18**, 29549–29554.
56. Lomzov,A.A., Sviridov,E.A., Shernuykov,A.V., Shevelev,G.Y., Pyshnyi,D.V. and Bagryanskaya,E.G. (2016) Study of a DNA duplex by nuclear magnetic resonance and molecular dynamics simulations. Validation of pulsed dipolar electron paramagnetic resonance distance measurements using triarylmethyl-based spin labels. *J. Phys. Chem. B*, **120**, 5125–5133.
57. Joseph,B., Tormyshev,V.M., Rogozhnikova,O.Y., Akhmetzyanov,D., Bagryanskaya,E.G. and Prisner,T.F. (2016) Selective high-resolution detection of membrane protein–ligand interaction in native membranes using trityl–nitroxide PELDOR. *Angew. Chem. Int. Ed.*, **55**, 11538–11542.
58. Jassoy,J.J., Berndhäuser,A., Duthie,F., Kühn,S.P., Hagelueken,G. and Schiemann,O. (2017) Versatile trityl spin labels for nanometer distance measurements on biomolecules in vitro and within cells. *Angew. Chem. Int. Ed.*, **56**, 177–181.
59. Krumkacheva,O. and Bagryanskaya,E. (2017) EPR-based distance measurements at ambient temperature. *J. Magn. Reson.*, **280**, 117–126.
60. Bobko,A.A., Kirilyuk,I.A., Grigor'ev,I.A., Zweier,J.L. and Khramtsov,V. V (2007) Reversible reduction of nitroxides to hydroxylamines: roles for ascorbate and glutathione. *Free Radical Biol. Med.*, **42**, 404–412.
61. Getz,E.B., Xiao,M., Chakrabarty,T., Cooke,R. and Selvin,P.R. (1999) A comparison between the sulfhydryl reductants tris (2-carboxyethyl) phosphine and dithiothreitol for use in protein biochemistry. *Anal. Biochem.*, **273**, 73–80.
62. Bagryanskaya,E.G., Trukhin,D.V., Troitskaya,T.I., Lomzov,A.A., Kuzhelev,A.A., Rogozhnikova,O.Y., Tormyshev,V.M., Pyshnyi,D.V., Fedin,M.V., Shevelev,G.Y. *et al.* (2014) Physiological-temperature distance measurement in nucleic acid using triarylmethyl-based spin labels and pulsed dipolar EPR spectroscopy. *J. Am. Chem. Soc.*, **136**, 9874–9877.
63. Jeschke,G., Chechik,V., Ionita,P., Godt,A., Zimmermann,H., Banham,J., Timmel,C.R., Hilger,D. and Jung,H. (2006) DeerAnalysis2006 - A comprehensive software package for analyzing pulsed ELDOR data. *Appl. Magn. Reson.*, **30**, 473–498.
64. Pannier,M., Veit,S., Godt,A., Jeschke,G. and Spiess,H.W. (2000) Dead-time free measurement of dipole–dipole interactions between electron spins. *J. Magn. Reson.*, **142**, 331–340.
65. Kanazhevskaya,L.Y., Koval,V.V., Lomzov,A.A. and Fedorova,O.S. (2014) The role of Asn-212 in the catalytic mechanism of human endonuclease APE1: stopped-flow kinetic study of incision activity on a natural AP site and a tetrahydrofuran analogue. *DNA Repair*, **21**, 43–54.
66. Lomzov,A.A., Vorobjev,Y.N. and Pyshnyi,D.V. (2015) Evaluation of the Gibbs free energy changes and melting temperatures of DNA/DNA duplexes using hybridization enthalpy calculated by molecular dynamics simulation. *J. Phys. Chem. B*, **119**, 15221–15234.
67. Shevelev,G.Y., Gulyak,E.L., Lomzov,A.A., Kuzhelev,A.A., Krumkacheva,O.A., Kupryushkin,M.S., Tormyshev,V.M., Fedin,M.V., Bagryanskaya,E.G. and Pyshnyi,D.V. (2018) A versatile approach to attachment of triarylmethyl labels to DNA for nanoscale structural EPR studies at physiological temperatures. *J. Phys. Chem. B*, **122**, 137–143.
68. Redrejo-Rodríguez,M., Vigouroux,A., Mursalimov,A., Grin,I., Alili,D., Koshenov,Z., Akishev,Z., Maksimenko,A., Bissenbaev,A.K. and Matkarimov,B.T. (2016) Structural comparison of AP endonucleases from the exonuclease III family reveals new amino acid residues in human AP endonuclease 1 that are involved in incision of damaged DNA. *Biochimie.*, **128**, 20–33.
69. Whitaker,A.M., Flynn,T.S. and Freudenthal,B.D. (2018) Molecular snapshots of APE1 proofreading mismatches and removing DNA damage. *Nat. Commun.*, **9**, 399.
70. Dyakonova,E.S., Koval,V.V., Lomzov,A.A., Ishchenko,A.A. and Fedorova,O.S. (2018) Apurinic/apyrimidinic endonuclease Apn1 from Saccharomyces cerevisiae is recruited to the nucleotide incision repair pathway: Kinetic and structural features. *Biochimie.*, **152**, 53–62.
71. Bode,B.E., Margraf,D., Plackmeyer,J., Dürner,G., Prisner,T.F. and Schiemann,O. (2007) Counting the monomers in nanometer-sized oligomers by pulsed electron– electron double resonance. *J. Am. Chem. Soc.*, **129**, 6736–6745.
72. Milov,A.D., Maryasov,A.G. and Tsvetkov,Y.D. (1998) Pulsed electron double resonance (PELDOR) and its applications in free-radicals research. *Appl. Magn. Reson.*, **15**, 107–143.
73. Moor,N.A., Vasil'eva,I.A., Anarbaev,R.O., Antson,A.A. and Lavrik,O.I. (2015) Quantitative characterization of protein–protein complexes involved in base excision DNA repair. *Nucleic Acids Res.*, **43**, 6009–6022.
74. Vasil'eva,I.A., Anarbaev,R.O., Moor,N.A. and Lavrik,O.I. (2019) Dynamic light scattering study of base excision DNA repair proteins and their complexes. *Biochim. Biophys. Acta* , **1867**, 297–305.
75. Yulikov,M. (2015) Spectroscopically orthogonal spin labels and distance measurements in biomolecules. In: Gilbert,BC, Chechik,V and Murphy,DM (eds). *Electron Paramagnetic Resonance*. The Royal Society of Chemistry, London, Vol. **24**, pp. 1–31.
76. Kuzhelev,A.A., Krumkacheva,O.A., Shevelev,G.Y., Yulikov,M., Fedin,M.V. and Bagryanskaya,E.G. (2018) Room-temperature distance measurements using RIDME and the orthogonal spin labels trityl/nitroxide. *Phys. Chem. Chem. Phys.*, **20**, 10224–10230.
77. Wilson,D.M. III and Barsky,D. (2001) The major human abasic endonuclease: formation, consequences and repair of abasic lesions in DNA. *Mutat. Res. Repair*, **485**, 283–307.
78. Dyrkheeva,N.S., Lebedeva,N.A. and Lavrik,O.I. (2016) AP endonuclease 1 as a key enzyme in repair of Apurinic/Apyrimidinic sites. *Biochem.*, **81**, 951–967.
79. Cuniasse,P., Fazakerley,G.V., Guschlbauer,W., Kaplan,B.E. and Sowers,L.C. (1990) The abasic site as a challenge to DNA polymerase: a nuclear magnetic resonance study of G, C and T opposite a model abasic site. *J. Mol. Biol.*, **213**, 303–314.
80. David-Cordonnier,M.-H., Cunniffe,S.M.T., Hickson,I.D. and O'Neill,P. (2002) Efficiency of incision of an AP site within clustered

DNA damage by the major human AP endonuclease. *Biochemistry*, **41**, 634–642.
81. Wilson,D.M. (2003) Properties of and substrate determinants for the exonuclease activity of human apurinic endonuclease Ape1. *J. Mol. Biol.*, **330**, 1027–1037.
82. Strauss,P.R., Beard,W.A., Patterson,T.A. and Wilson,S.H. (1997) Substrate binding by human apurinic/apyrimidinic endonuclease indicates a Briggs-Haldane mechanism. *J. Biol. Chem.*, **272**, 1302–1307.
83. Wilson,D.M., Takeshita,M. and Demple,B. (1996) Abasic site binding by the human apurinic endonuclease, Ape, and determination of the DNA contact sites. *Nucleic Acids Res.*, **25**, 933–939.
84. Masuda,Y., Bennett,R.A.O. and Demple,B. (1998) Rapid dissociation of human apurinic endonuclease (Ape1) from incised DNA induced by magnesium. *J. Biol. Chem.*, **273**, 30360–30365.